CHAPTER IV
RESULTS AND DISCUSSION

4.1 Adsorbent Characterization

4.1.1 Characterization of Adsorbent by Nitrogen Adsorption/desorption Method and Mercury Porosimetry

By using Nitrogen adsorption/desorption at 77K and Mercury porosimetry methods, properties of the adsorbents used in this study are presented in Tables 4.1 and 4.2 for specific surface area and pore structure.

Table 4.1 Properties of adsorbents by using the nitrogen adsorption/desorption methods at 77K

Adsorbent	BET Surface area (m^2/g)	V_μ (t-plot) (cm^3/g)	V_{BJH} (B.J.H.) (cm^3/g)	V_m (P/P_0=0.99) (cm^3/g)	$V_m + V_\mu$ (cm^3/g)
Mesoporous alumina (70333)	278	0.000	0.748	0.752	0.752
Macroporous alumina (70337)	194	0.000	0.520	0.523	0.523
Activated carbon (69597)	1263	0.242	0.255	0.392	0.634
Mesoporous alumina (D = 0.1-0.4 mm) (76911)	281	0.003	0.759	0.751	0.754
Macroporous alumina (D = 0.1-0.4 mm) (76913)	191	0.001	0.532	0.533	0.534
$CuCl_2/H_2O$ impregnated on mesoporous alumina (75226)	137	0.002	0.416	0.414	0.416

Table 4.1 (cont.) Properties of adsorbents by using the nitrogen adsorption/desorption methods at 77K

Adsorbent	BET Surface area (m^2/g)	V_μ (t-plot) (cm^3/g)	V_m (B.J.H.) (cm^3/g)	V_m (P/P_0=0.99) (cm^3/g)	$V_m + V_\mu$ (cm^3/g)
$CuCl_2/H_2O$ impregnated on macroporous alumina (75228)	108	0.002	0.328	0.325	0.328
$CuCl_2/H_2O$ impregnated on activated carbon (75850)	743	0.127	0.066	0.377	0.504
$CuCl_2/H_2O$ impregnated on mesoporous alumina (D = 0.1-0.4 mm) (77118)	229	0.000	0.549	0.563	0.563
$CuCl_2/H_2O$ impregnated on macroporous alumina (D = 0.1-0.4 mm) (77121)	161	0.000	0.399	0.408	0.408
CuCl/75%CH_3CN-25%H_2O impregnated on mesoporous alumina (D = 0.1-0.4 mm) (77117)	208	0.000	0.522	0.529	0.529
CuCl/75%CH_3CN-25%H_2O impregnated on macroporous alumina (D = 0.1-0.4 mm) (77119)	149	0.000	0.396	0.396	0.396
$NiCl_2/H_2O$ impregnated on mesoporous alumina (75227)	213	0.000	0.517	0.530	0.530

Table 4.1 (cont.) Properties of adsorbents by using the nitrogen adsorption/desorption methods at 77K

Adsorbent	BET Surface area (m^2/g)	V_μ (t-plot) (cm^3/g)	V_m (B.J.H.) (cm^3/g)	V_m (P/P_0=0.99) (cm^3/g)	$V_m + V_\mu$ (cm^3/g)
$NiCl_2/H_2O$ impregnated on macroporous alumina (75229)	163	0.000	0.387	0.396	0.396
$NiCl_2/H_2O$ impregnated on mesoporous alumina (D = 0.1-0.4 mm) (77258)	262	0.000	0.643	0.654	0.654

Table 4.2 Properties of adsorbents by using the Mercury porosimetry

Adsorbent	Particle density (g/cm^3)	Structural density (g/cm^3)	V_m (cm^3/g)	V_M (cm^3/g)	$V_m + V_M$ (cm^3/g)
Mesoporous alumina (70333)	0.914	2.806	0.643	0.009	0.652
Macroporous alumina (70337)	1.008	2.994	0.481	0.151	0.632
Activated carbon (69597)	0.653	1.090	0.138	0.390	0.528
Mesoporous alumina (D = 0.1-0.4 mm) (76911)	0.482	2.306	0.670	0.036	0.706
Macroporous alumina (D = 0.1-0.4 mm) (76913)	0.557	2.835	0.455	0.131	0.586
$CuCl_2/H_2O$ impregnated on mesoporous alumina (75226)	1.202	3.091	0.471	0.008	0.480

Table 4.2 (cont.) Properties of adsorbents by using the Mercury porosimetry

Adsorbent	Particle density (g/cm^3)	Structural density (g/cm^3)	V_m (cm^3/g)	V_M (cm^3/g)	$V_m + V_M$ (cm^3/g)
$CuCl_2/H_2O$ impregnated on macroporous alumina (75228)	1.183	3.142	0.367	0.129	0.496
$CuCl_2/H_2O$ impregnated on activated carbon (75850)	0.794	1.036	0.168	0.075	0.243
$CuCl_2/H_2O$ impregnated on mesoporous alumina (D = 0.1-0.4 mm) (77118)	0.326	0.588	0.456	0.019	0.475
$CuCl_2/H_2O$ impregnated on macroporous alumina (D = 0.1-0.4 mm) (77121)	0.593	2.380	0.374	0.092	0.467
CuCl/75%CH_3CN-25%H_2O impregnated on mesoporous alumina (D = 0.1-0.4 mm) (77117)	0.661	3.058	0.431	0.017	0.449
CuCl/75%CH_3CN-25%H_2O impregnated on macroporous alumina (D = 0.1-0.4 mm) (77119)	0.710	3.871	0.368	0.098	0.466
$NiCl_2/H_2O$ impregnated on mesoporous alumina (75227)	1.019	2.874	0.543	0.007	0.549

Table 4.2 (cont.) Properties of adsorbents by using the Mercury porosimetry

Adsorbent	Particle density (g/cm^3)	Structural density (g/cm^3)	V_m (cm^3/g)	V_M (cm^3/g)	$V_m + V_M$ (cm^3/g)
$NiCl_2/H_2O$ impregnated on macroporous alumina (75229)	1.071	2.740	0.406	0.133	0.539
$NiCl_2/H_2O$ impregnated on mesoporous alumina (D = 0.1-0.4 mm) (77258)	0.575	2.739	0.545	0.009	0.554

Where V_μ = microporous volume

V_m = mesoporous volume

V_M = macroporous volume

According to Table 4.1, the BET surface area and porous volume of Cu^{2+} impregnated on mesoporous and macroporous alumina is lower than Ni^{2+} impregnated on alumina and pure alumina respectively. Since the metals, Cu and Ni, cover on the surface of adsorbent, the surface area is decreased.

From Table 4.2, particle density of Cu^{2+} impregnated on mesoporous alumina is higher than Ni^{2+} impregnated on mesoporous alumina and pure mesoporous alumina respectively because Cu has higher molecular weight than Ni. For macroporous alumina, they show the same trend as the mesoporous alumina.

4.1.2 Temperature-Programmed Reduction

4.1.2.1 Temperature-Programmed Reduction of $CuCl_2$ Impregnated on the Adsorbent

Since a CuCl is difficult to solute in water, Cu^+ adsorbent was prepared by the incipient wetness method of $CuCl_2$ on the adsorbent, followed by reduction to convert Cu^{2+} to Cu^+. To understand its reduction behavior, $CuCl_2$ impregnated on mesoporous alumina was first heated in a flow 10% H_2 in Ar up to 900°C at a heating rate of 5 °C/min. The intensity measured by thermal conductivity detector (TCD) indicated H_2 consumption. The result is shown in Figure 4.1. During the heat treatment of $CuCl_2$ in H_2, two distinct peaks, at 278°C and 435°C, were detected. These two peaks correspond to two reduction steps. The first peak at 278°C indicates the reduction from Cu^{2+} to Cu^+, and the second peak indicates the reduction from Cu^+ to Cu^0. From above result, it is determined that 278°C is the appropriate temperature for reduction to Cu^+. The intensity change of TCD detector during the reduction of Cu^{2+} is shown in Figure 4.2. The intensity at 278°C began to decrease after 2 hours, indicating that most of Cu^{2+} was converted to Cu^+. Subsequently, Cu^{2+} impregnated on the adsorbents was reduced at 278°C for 1 hour in presence of H_2. The above results agree with the results from the study of Takahashi (2000) that studied the reduction of $CuCl_2/Al_2O_3$ where they observed 2 distinct peaks at 270 and 410°C. They also concluded that the first peak corresponded to the reduction of Cu^{2+} to Cu^+ and the second peak corresponded to the reduction of Cu^+ to Cu^0.

From Table 4.3, hydrogen consumption is 1.727 mmol of H_2/g of adsorbent that corresponds with 1.797 mmol of Cu/g of adsorbent from atomic absorption spectroscopy (AAS) result. It means that 1 mole of H_2 can react with 1 mole of $CuCl_2$. It can be interpreted in chemical equation as follow:

$$CuCl_2 + \frac{1}{2}H_2 \rightarrow CuCl + HCl \qquad (4.1)$$

$$CuCl + \frac{1}{2}H_2 \rightarrow Cu + HCl \qquad (4.2)$$

$$CuCl_2 + H_2 \rightarrow Cu + 2HCl \quad (4.3)$$

Table 4.3 Hydrogen consumption measured in TPR measurement for Cu

Peak number	Temperature	H_2 Volume (mmol/g)
1	278.4	0.864
2	435.3	0.863
Total hydrogen consumption		1.727

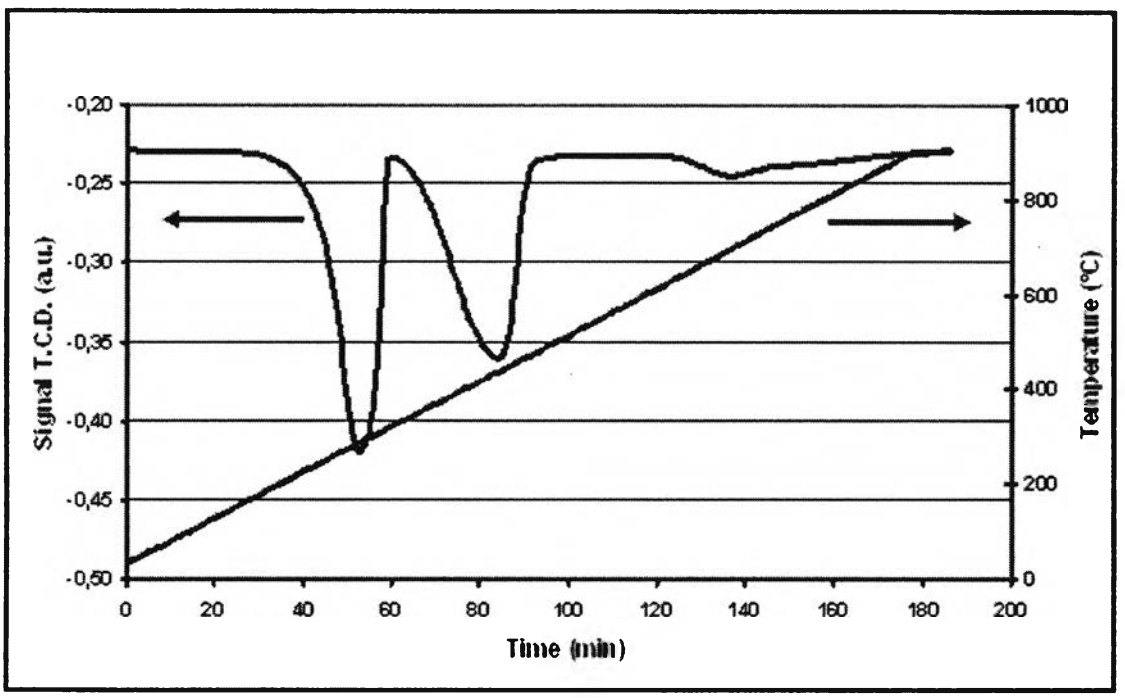

Figure 4.1 Temperature-programmed reduction (TPR) of $CuCl_2$ impregnated on mesoporous alumina in 10% H_2 in Ar.

Other two samples were reduced under pure H_2 and He to obtain Cu^+ with a gas flow rate of 37 cm^3/min and 300°C to get a complete reduction. Then, they were sent to analyze by temperature-programmed reduction. The TPR result, as

shown in Figure 4.3, of Cu^{+} reduced by H_2 indicates that the first peak is almost disappeared and the second peak is still remaining. It can be concluded that it was suitable to use H_2 at 37 cm^3/min and heated from ambient temperature to 300°C to obtain Cu^{+}. The temperature and H_2 volume consumption of each peak is shown in Table 4.4.

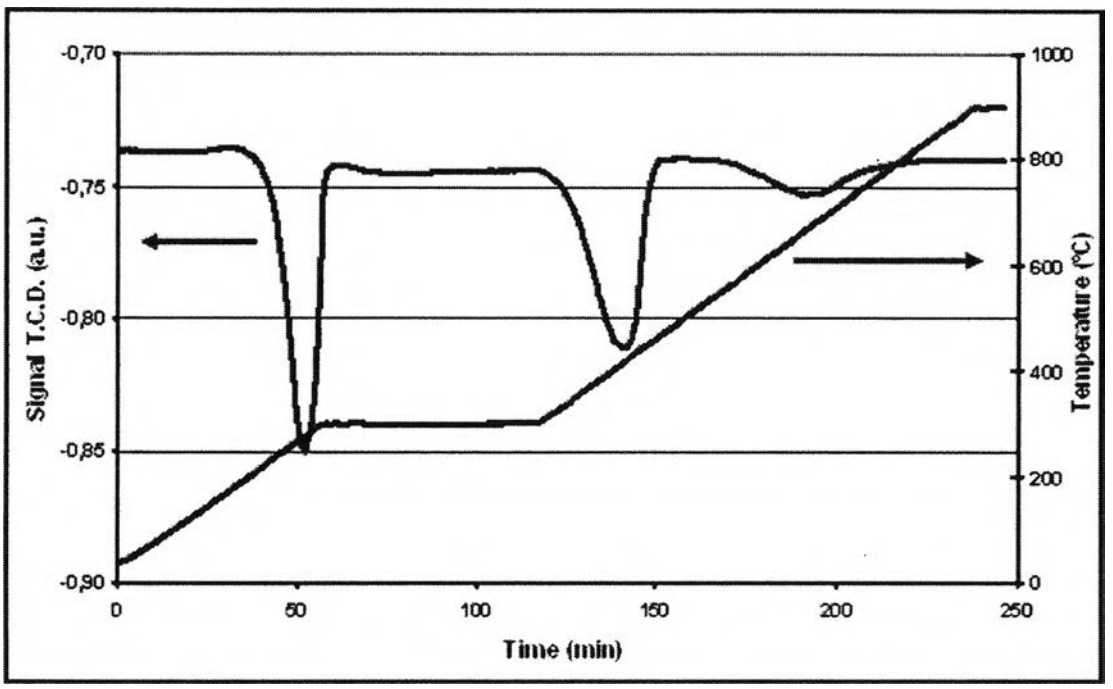

Figure 4.2 Temperature-programmed reduction (TPR) of $CuCl_2$ impregnated on mesoporous alumina in 10% H_2 in Ar.

Table 4.4 Hydrogen consumption measured in TPR measurement for $CuCl_2$ reduced under H_2

Peak number	Temperature	H_2 Volume (mmol/g)
1	231.9	0.068
2	410.9	0.692
Total hydrogen consumption		0.760

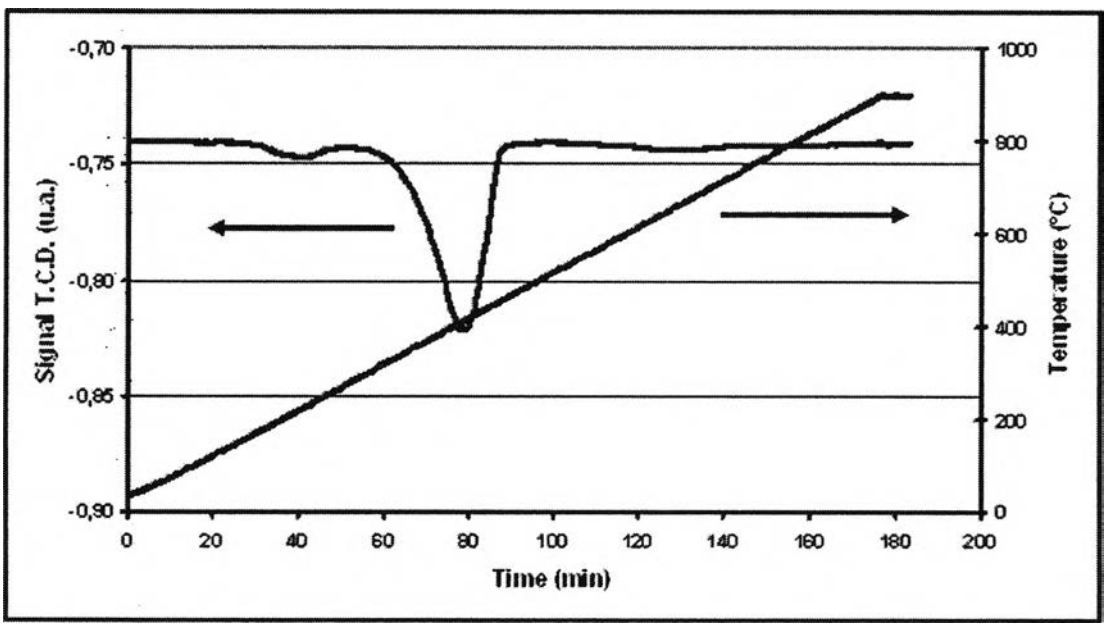

Figure 4.3 Temperature-programmed reduction (TPR) of $CuCl_2$ impregnated on mesoporous alumina reduced by H_2.

Figure 4.4 shows TPR result and Table 4.5 shows reduction temperature and H_2 consumption from $CuCl_2$ reduced by He. From this result, it can be observed that there are two peaks occurring at almost the same temperature with $CuCl_2$ without reduction (Figure 4.1). It can be mentioned that He cannot reduce Cu^{2+} to Cu^{+}.

Table 4.5 Hydrogen consumption measured in TPR measurement for $CuCl_2$ reduced under He

Peak number	Temperature	H_2 Volume (mmol/g)
1	294.3	0.988
2	439.0	1.007
Total hydrogen consumption		1.995

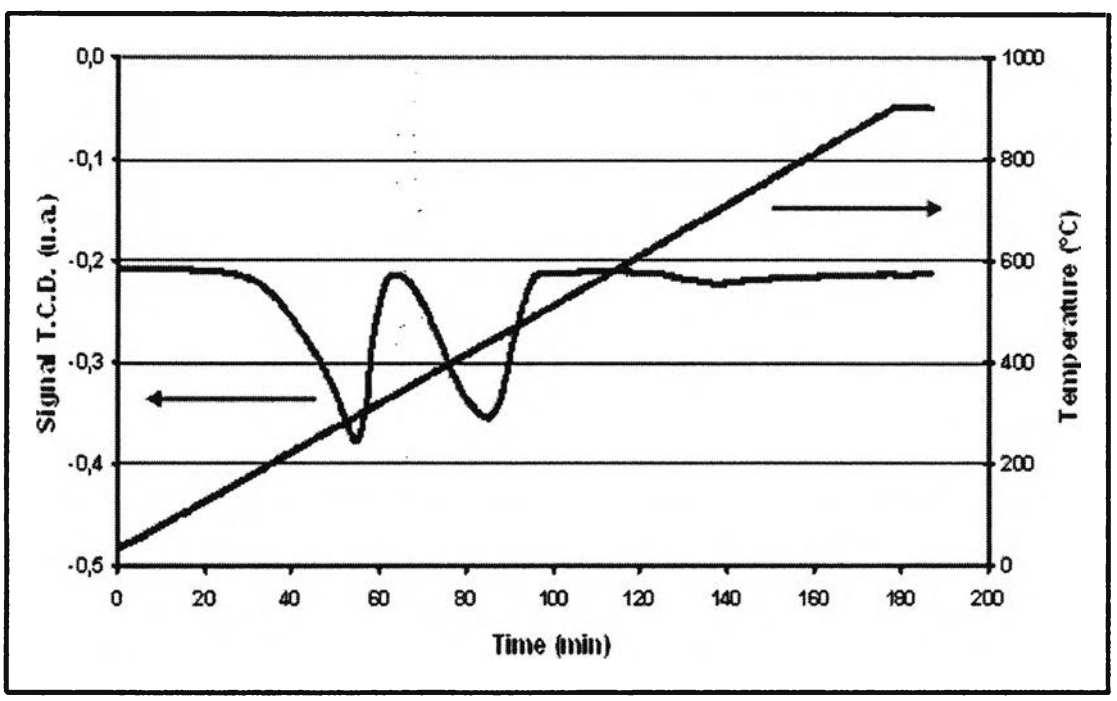

Figure 4.4 Temperature-programmed reduction (TPR) of $CuCl_2$ impregnated on mesoporous alumina "reduced" by He

4.1.2.2 Temperature-Programmed Reduction of CuCl in 75% Acetonitrile-25% Deionized Water Impregnated on the Adsorbent

There was another way to obtain Cu^+ directly by using CuCl dissolved in acetronitrile solution. CuCl in 75% acetonitrile-25% deionized water

impregnated on mesoporous alumina was analyzed in the same condition as previous. The result is shown in Figure 4.5 and Table 4.6. During the heat treatment in H_2, two distinct peaks, at 271°C and 396°C, were detected. These two peaks correspond to two reduction steps. The first peak at 271°C indicates the reduction from Cu^{2+} to Cu^{+}, and the second peak indicates the reduction from Cu^{+} to Cu^{0}. Form this result, it can be mentioned that this method of preparation CuCl in 75% acetonitrile-25% deionized water is not successful because the presence of Cu^{2+} is observed, since the cuprous solution was very easy to be oxidized to Cu^{2+} even just by being exposed to the air. Even though the synthesis process handled with special care to avoid this transformation, this preparation method is not convenient because the adsorbent was impregnated several times to obtain the monolayer coverage.

Table 4.6 Hydrogen consumption measured in TPR measurement for CuCl

Peak number	Temperature	H_2 Volume (mmol/g)
1	271.1	1.491
2	395.9	0.858
Total hydrogen consumption		2.349

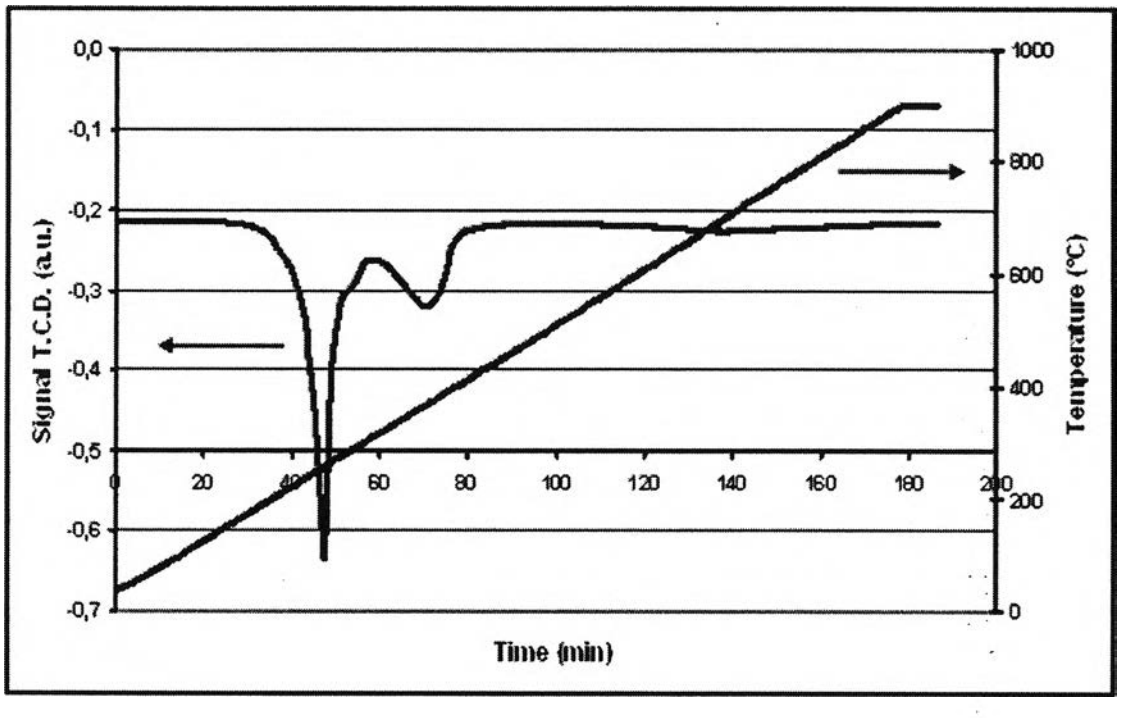

Figure 4.5 Temperature-programmed reduction (TPR) of CuCl in 75% cetonitrile-25% deiornized water impregnated on mesoporous in 10% H_2 in Ar.

4.1.2.3 Temperature-Programmed Reduction of $NiCl_2$ Impregnated on the Adsorbent

$NiCl_2$ impregnated on mesoporous alumina was analyzed in the same condition as $CuCl_2$. During the heat treatment of $NiCl_2$ in H_2 at 450°C was detected. This peak corresponded to one reduction step from Ni^{2+} to Ni^0. From Table 4.7, hydrogen consumption is 1.063 mmol of H_2/g of adsorbent that corresponds with 1.021 mmol of Ni/g of adsorbent from AAS result. It mean that 1 mole of H_2 can react with 1 mole of $NiCl_2$. It can be interpreted in chemical reaction as follow:

$$NiCl_2 + H_2 \rightarrow Ni + 2HCl \qquad (4.4)$$

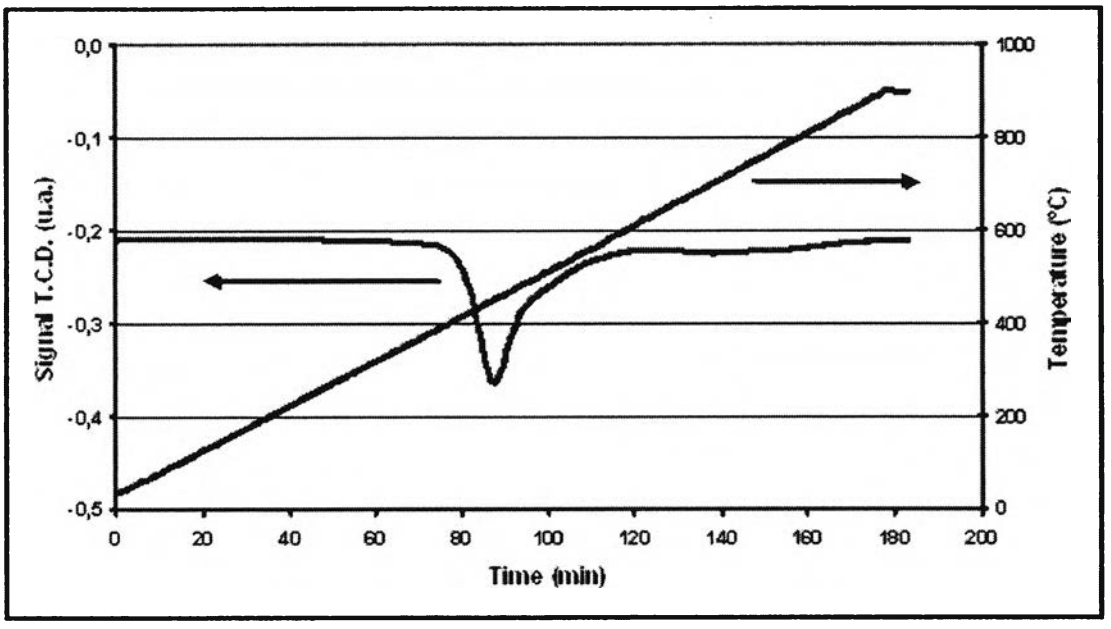

Figure 4.6 Temperature-programmed reduction (TPR) of $NiCl_2$ impregnated on mesoporous alumina in 10% H_2 in Ar.

Table 4.7 Hydrogen consumption measured in TPR measurement for $NiCl_2$

Peak number	Temperature	H_2Volume (mmol/g)
1	450.4	1.063
Total hydrogen consumption		1.063

4.2 Fixed-Bed Adsorption Experiments

After activation (or reduction) of non-impregnated or impregnated adsorbent, the simulated diesel fuel feed (150 ppmw S) was allowed to contact the adsorbent bed and the effluent total sulfur content monitored periodically. The dead volume of the lines before and after the fixed-bed reactor was also determined in order to evaluate the cumulative effluent volume. The adsorption amounts were obtained after intergrating the

area above the breakthrough curves. Breakthrough adsorption curves were generated by ploting the transient total sulfur concentration normalized by the feed total sulfur concentration versus cumulative fuel volume.

4.2.1 Effect of Feed Flow Rate on the Sulfur Adsorption Capacites

To observe the effect of the feed flow rate, experiments were conducted at 2 and 0.4 cm^3/min. They were examined for removal sulfur compounds at 30°C. Figure 4.7 shows the resulting breakthrough curves for Ni^{2+} impregnated on mesoporous alumina at 2 and 0.4 cm^3/min and Table 4.8 summarizes the results obtained from the breakthrough and adsorption capacities.

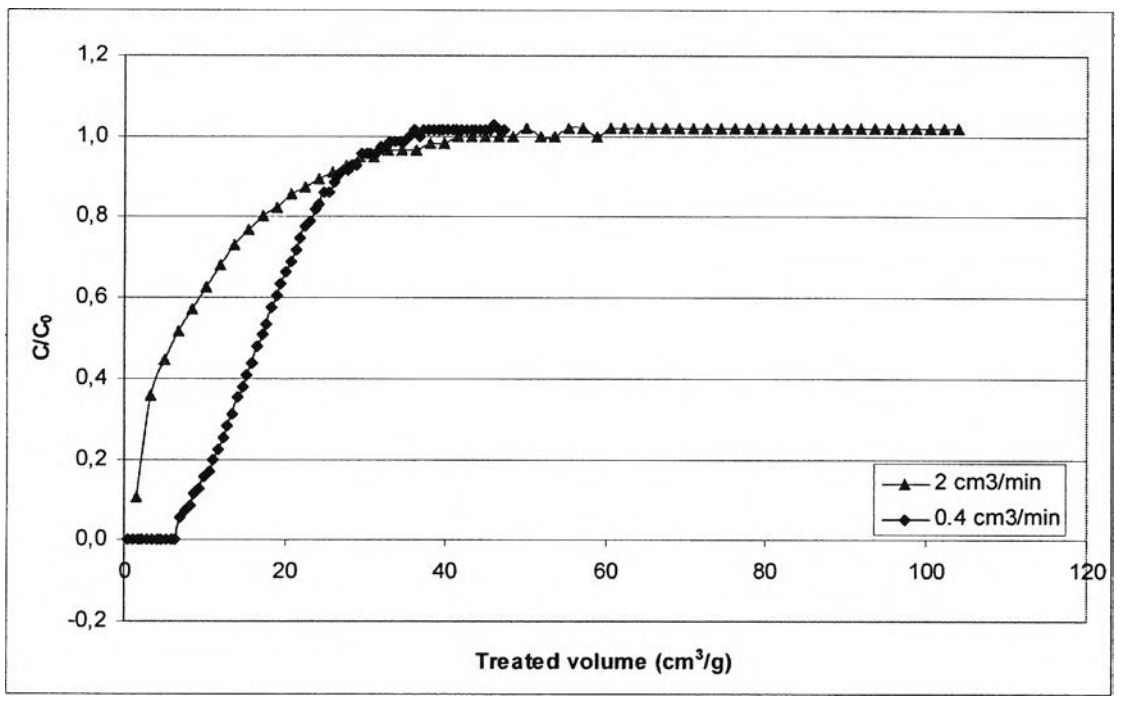

Figure 4.7 Breakthrough curve of dibenzothiophene in a fixed-bed adsorber over Ni^{2+} impregnated on mesoporous alumina at 2 cm^3/min (▲) and 0.4 cm^3/min (♦).

Table 4.8 Breakthrough and adsorption capacities loading for dibenzothiophene from simulated diesel fuel in Ni^{2+} impregnated on mesoporous alumina at different feed flow rates

Feed flow rate	Breakthrough capacity (mmol/g)	Adsorption capacity (mmol/g)
2 cm^3/min	0.0000	0.0250
0.4 cm^3/min	0.0093	0.0555

The higher feed flow rate showed higher both breakthrough and adsorption capacities than the lower feed flow rate. The breakthrough and adsorption capacities of dibenzothiophene at flow rate of 0.4 cm^3/min were 0.0093 and 0.0250 mmol DBT/g, respectively. The higher feed flow rate showed higher breakthrough capacities since at low feed flow rate, the dibenzothiophene had longer time to contact the surface of the adsorbent. Thus the dibenzothiophene could be more adsorbed.

4.2.2 Influence of Adsorbent Granulometry on the Sulfur Adsorption Capacities

To understand the influence of adsorbent granulometry on the sulfur adsorption capacity, two different diameter sizes of Ni^{2+} impregnated on mesoporous alumina adsorbents were used. The diameter sizes of these adsorbents were 4 mm and 100-400 μm. They were examined for removal sulfur compounds by breakthrough experiments at flow rate 0.4 cm^3/min and 30°C. Figure 4.8 shows the resulting breakthrough curves for the Ni^{2+} impregnated on mesoporous in size of 4 mm and 100-400 μm and Table 4.9 summarizes the results obtained from the breakthrough and adsorption capacities.

Table 4.9 Breakthrough and adsorption capacities loading for dibenzothiophene from simulated diesel fuel in Ni^{2+} impregnated on mesoporous alumina in different sizes of adsorbents

Granulometry size	Breakthrough capacity (mmol/g)	Adsorption capacity (mmol/g)
4 mm	0.0093	0.0250
100-400 μm	0.0123	0.0216

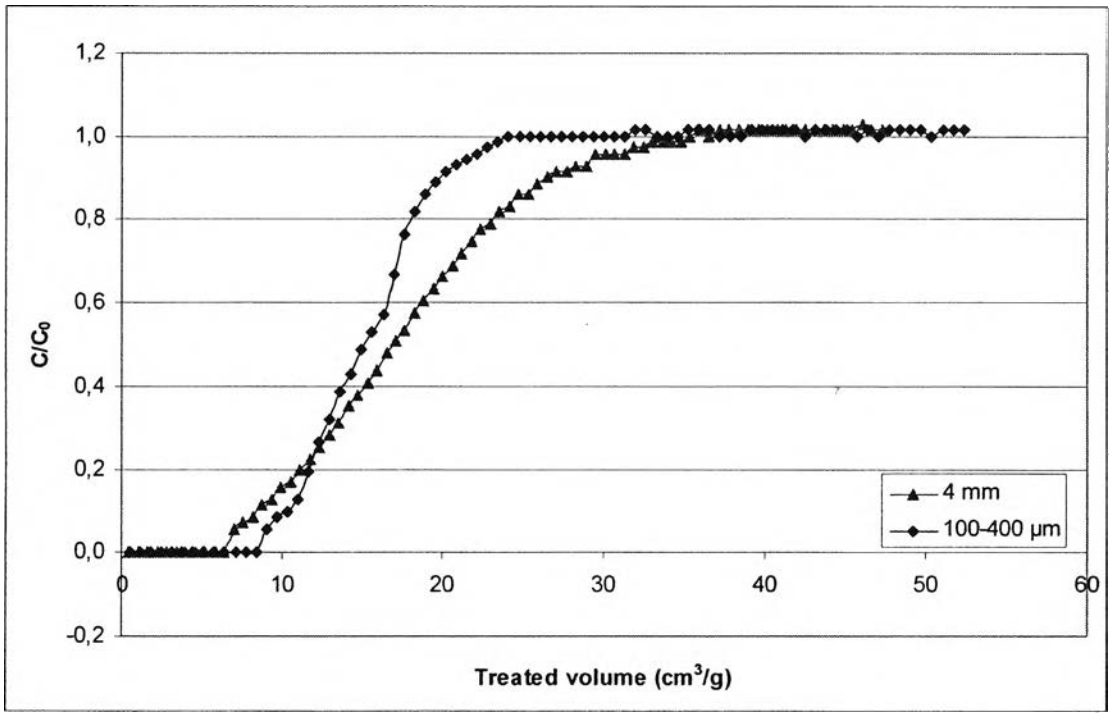

Figure 4.8 Breakthrough curve of dibenzothiophene in a fixed-bed adsorber over Ni^{2+} impregnated on mesoporous alumina in size of 4 mm (▲) and 100-400 μm (♦).

From Figure 4.8 and Table 4.9, the adsorbent that had 100-400 μm for diameter size showed higher breakthrough capacities than the adsorbent that had 4 mm

for diameter size. The breakthrough capacities of dibenzothiophene were 0.0123 mmol DBT/g, indicating higher amount of sulfur adsorbed. The lower breakthrough capacity of 4mm diameter size adsorbent could be due to the internal mass transfer limitation.

4.2.3 Influence of Adsorption Temperature on the Sulfur Adsorption Capacities

Since the kinetics of adsorption can be affected by adsorption temperature, the influence of adsorption temperature on the adsorption capacities with two different types of adsorbents, Ni^{2+} and Cu^{+} impregnated on mesoporous alumina at 0.4 cm^3/min of feed flow rate and 100-400 μm of diameter size was examined.

For Ni^{2+} impregnated on mesoporous alumina, it was carried out at two adsorption temperatures that are 30°C and 60°C. The results from these two breakthrough experiments are shown in Figure 4.9. Table 4.10 summarises the results for breakthrough and adsorption capacities.

Table 4.10 Breakthrough and adsorption capacities loading for dibenzothiophene from simulated diesel fuel in Ni^{2+} impregnated on mesoporous alumina with different adsorption temperatures

Adsorption temperature	Breakthrough capacity (mmol/g)	Adsorption capacity (mmol/g)
30°C	0.0123	0.0216
60°C	0.0199	0.0243

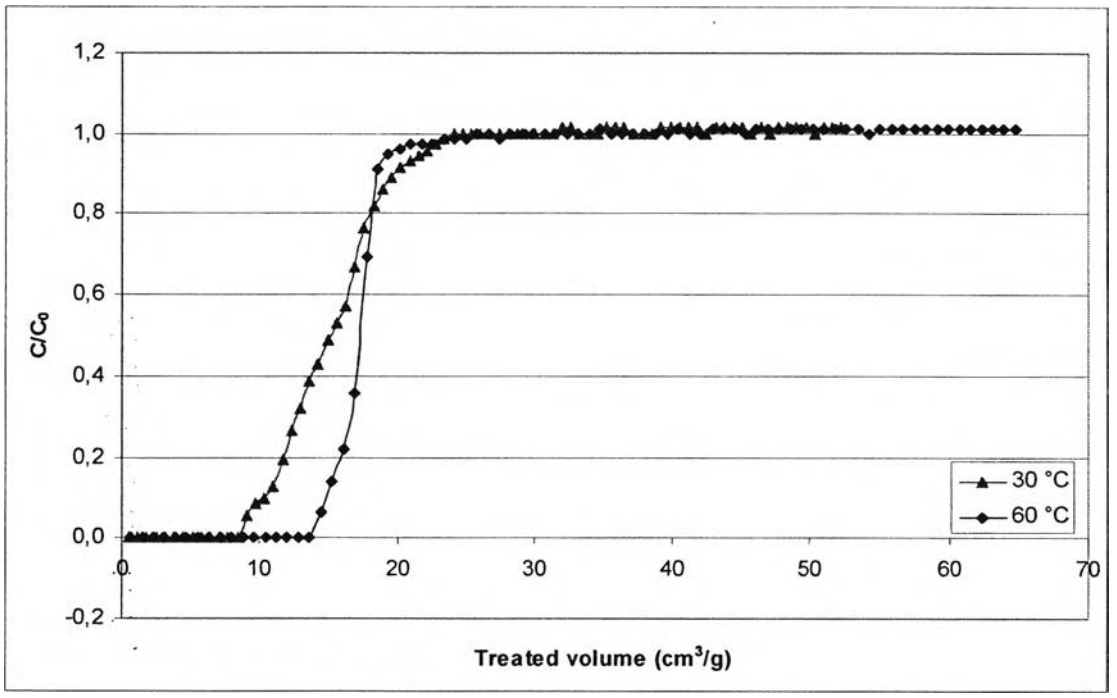

Figure 4.9 Breakthrough curve of dibenzothiophene in a fixed-bed adsorber over Ni^{2+} impregnated on mesoporous alumina with adsorption temperature at 30°C (▲) and 60°C (♦).

From Figure 4.9 and Table 4.10, the breakthrough experiment at 60°C showed higher both breakthrough and adsorption capacities than the breakthrough experiment at 30°C. The breakthrough and adsorption capacities at 60°C were 0.0198 and 0.0241 mmol DBT/g, respectively. These results indicate a higher kinetic adsorption due to higher adsorption temperature in agreement with the Arrhenius law. Thus the adsorption temperature at 60°C is suitable for the sulfur adsorption with Ni^{2+} impregnated on the adsorbents.

Since the above results, Cu^{+} impregnated on mesoporous alumina was examined, at 60°C and 90°C with 0.4 cm^3/min of feed flow rate and 100-400 μm of diameter size. The results from these two breakthrough experiments are shown in Figure 4.10. Table 4.11 summarises the results from breakthrough and adsorption capacities.

Table 4.11 Breakthrough and adsorption capacities loading for dibenzothiophene from simulated diesel fuel in Cu^{+} impregnated on mesoporous alumina with different adsorption temperatures

Adsorption temperature	Breakthrough capacity (mmol/g)	Adsorption capacity (mmol/g)
60°C	0.0026	0.0147
90°C	0.0078	0.0089

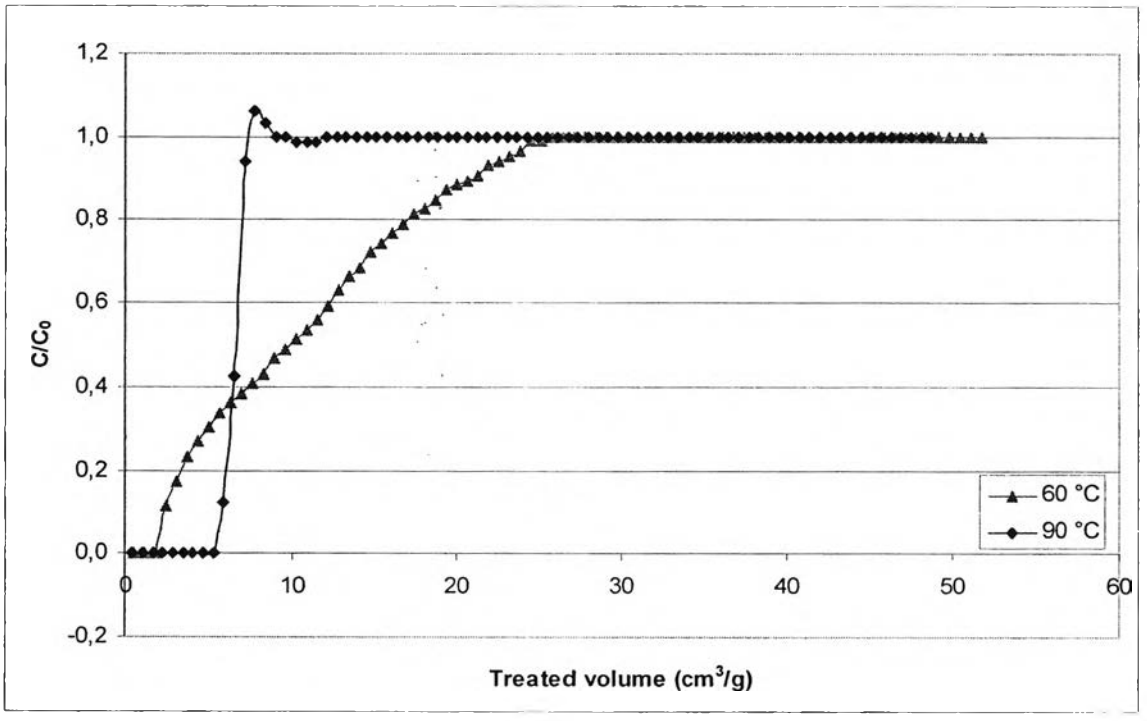

Figure 4.10 Breakthrough curve of dibenzothiophene in a fixed-bed adsorber over Cu^{+} impregnated on mesoporous alumina with adsorption temperature at 60°C (▲) and 90°C (♦).

From Figure 4.10 and Table 4.11, the breakthrough and adsorption capacities for the experiment at 60 °C were 0.0026 and 0.0146 mmol DBT/g, respectively and the breakthrough and adsorption capacities for the experiment at 90 °C were 0.0078 and 0.0089 mmol DBT/g, respectively. It can be mentioned that the breakthrough experiment at 90°C can produce more sulfur-free effluent than the breakthrough experiment at 60°C, while the breakthrough experiment at 60°C can adsorb dibenzothiophene more than the breakthrough experiment at 90°C. Again, the influence of the temperature on the adsorption kinetics is clearly shown, with a less broad curve at 90°C than at 60°C. Thus the suitable adsorption temperature for Cu^{+} impregnated on the adsorbents is 90°C.

An interesting phenomenon found in the breakthrough experiment at 90°C is that after breakthrough, the C/C_0 value (a ratio of the outlet concentration to the initial concentration in simulated diesel) increased sharply to over 1.0. After passing the maximum value, the outlet concentration decreased gradually to the initial one. It can be inferred from this phenomenon that the adsorption of such compounds is at least partially reversible.

4.2.4 Effect of Different Adsorbents on the Sulfur Adsorption Capacities

Adsorption performance of the adsorbents usually depends on both surface area chemical property, such as active sites and their density, and physical property, including surface area, pore size and distribution. Thus, to observe the sulfur adsorption capacities of different adsorbents, 8 types of adsorbents were used in these experiments that were non-impregnated activated carbon, non-impregnated mesoporous alumina, non-impregnated macroporous alumina, Ni^{2+} impregnated on mesoporous alumina, Ni^{2+} impregnated on macroporous alumina, Cu^{+} impregnated on mesoporous alumina, Cu^{+} impregnated on macroporous alumina and Cu^{+} impregnated on activated carbon. All of the experiments were carried out at 0.4 cm^3/min, 60°C and 100-400 μm of diameter size. Figure 4.11 shows the resulting breakthrough curves for different adsorbents and Table 4.12 summarizes the results obtained from the breakthrough and adsorption capacities.

The results show that the adsorptive capacities (both breakthrough and adsorption capacities) based on the adsorbent weight increase in the order of non-impregnated macroporous alumina < Cu^{+} impregnated on macroporous alumina < non-impreganted mesoporous alumina < Cu^{+} impregnated on mesoporous alumina < Ni^{2+} impregnated on macroporous alumina < Ni^{2+} impregnated on mesoporous alumina < Cu^{+} impregnated on activated carbon < non-impregnated activated carbon. The non-impregnated activated carbon is the best adsorbent among 8 adsorbents due to it has about 8 times higher surface area than other adsorbents, as shown in Table 4.1. The breakthrough capacity of Cu^{+} impregnated on activated carbon was 0.0448 mmol DBT/g. Although this capacity is relatively high compared with others, it is less than that observed with non-impregnated activated carbon. It can be explained by the study of Han and co-workers (2003) that at high %Cu loading on the activated carbon, the conglomerate of $CuCl_2$ formed by impregnation of excessive $CuCl_2$ and active sites are also formed in multi-layer, not monolayer.

Table 4.12 Breakthrough and adsorption capacities loading for dibenzothiophene from simulated diesel fuel with different adsrobents

Adsorbent	Breakthrough capacity (mmol/g)	Adsorption capacity (mmol/g)
Non-impregnated activated carbon	0.1343	0.1564
Non-impregnated mesoporous alumina	0.0010	0.0110
Non-impregnated macroporous alumina	0.0000	0.0023
Ni^{2+} impregnated on mesoporous alumina	0.0199	0.0243
Ni^{2+} impregnated on macroporous alumina	0.0151	0.0160
Cu^{+} impregnated on mesoporous alumina	0.0026	0.0147
Cu^{+} impregnated on macroporous alumina	0.0007	0.0096
Cu^{+} impregnated on activated carbon	0.0448	0.0550

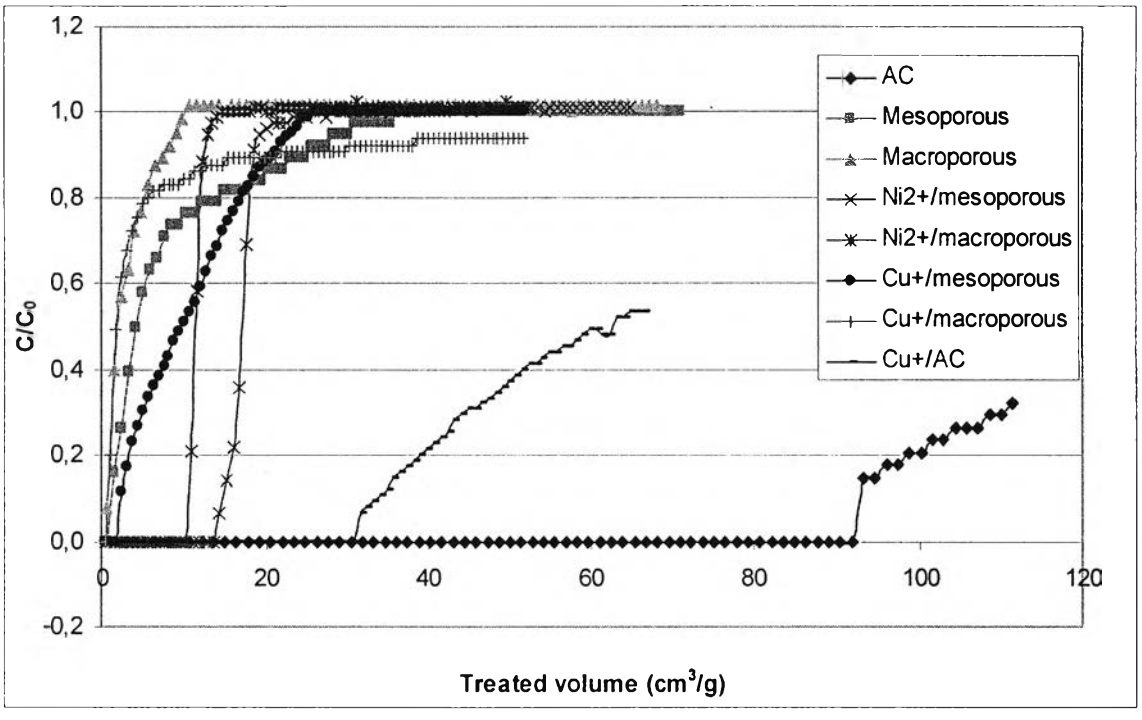

Figure 4.11 Breakthrough curve of dibenzothiophene in a fixed-bed adsorber over non-impregnated activated carbon (♦), non-impregnated mesoporous alumina (■), non-impregnated macroporous alumina (▲), Ni^{2+} impregnated on mesoporous alumina (x), Ni^{2+} impregnated on macroporous alumina (✶), Cu^{+} impregnated on mesoporous alumina (●), Cu^{+} impregnated on macroporous alumina (|) and Cu^{+} impregnated on activated carbon (-).

4.2.5 Influence of Cu Charge on the Sulfur Adsorption Capacities

To study the influence of Cu charge on the sulfur adsorption capacities, three different types of adsorbents were observed: (1) Cu^{2+} impregnated on mesoporous alumina without reduction; (2) Cu^{2+} impregnated on mesoporous alumina reduced by using He; (3) Cu^{2+} impregnated on mesoporous alumina reduced by using H_2. These experiments were carried out at 2 cm^3/min of feed flow rate and 30°C.

Figure 4.12 showed the sulfur breakthrough curves for simulated diesel fuel over Cu^{2+} impregnated on mesoporous alumina without reduction, with reduction

by He, and reduction by H_2 and Table 4.13 summarizes the results obtained for the breakthrough and adsorption capacities.

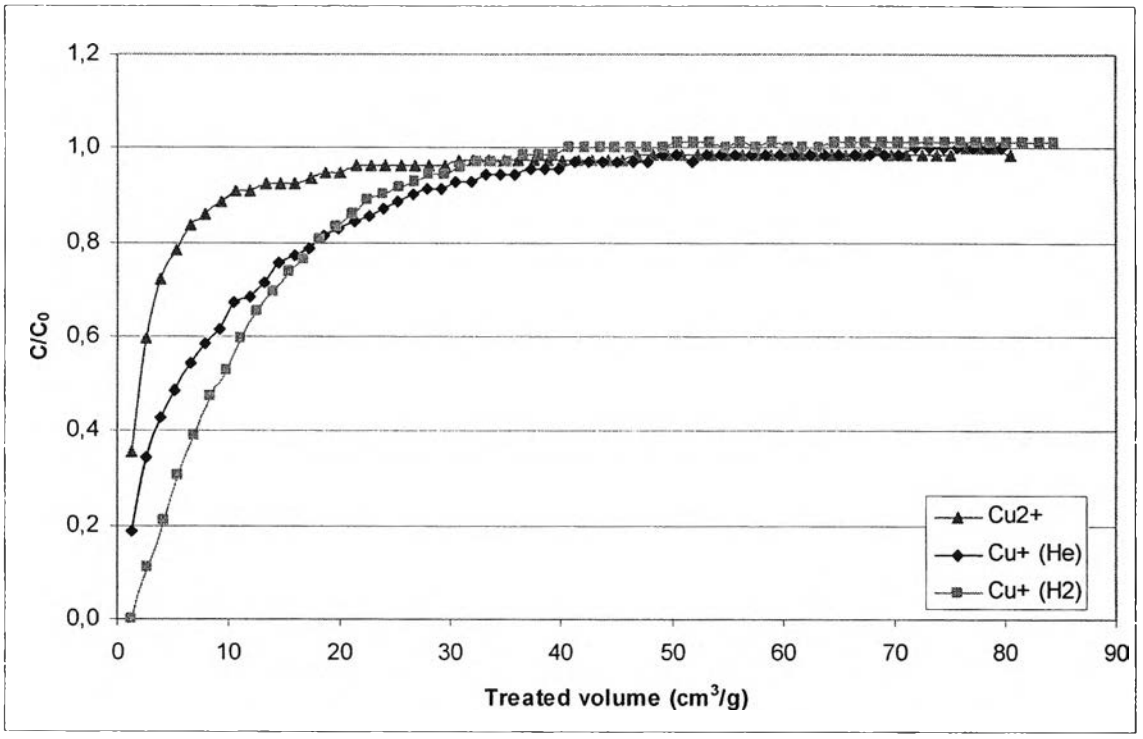

Figure 4.12 Breakthrough curve of dibenzothiophene in a fixed-bed adsorber over Cu^{2+} impregnated on mesoporous alumina without reduction (▲), reduction by He (♦), and reduction by H_2 (■).

Table 4.13 Breakthrough and adsorption capacities loading for dibenzothiophene from simulated diesel fuel in Cu^{2+} impregnated on mesoporous alumina

Cu^{2+} impregnated on mesoporous alumina	Breakthrough capacity (mmol/g)	Adsorption capacity (mmol/g)
Without reduction	0.0000	0.0262
Reduction by He	0.0000	0.0687
Reduction by H_2	0.0095	0.0754

From Table 4.13, the breakthrough capacities of Cu^{2+} impregnated on mesoporous alumina without reduction and Cu^{+} impregnated on mesoporous alumina reduced by He were zero mmol DBT/g, while breakthrough capacities of Cu^{+} impregnated on mesoporous alumina reduced by H_2 was 0.0095 mmol of DBT/g of adsorbent. It can be concluded that Cu^{+} reduced by H_2 possesses stronger affinity with DBT via π-complexation bond than Cu^{2+}. This is a clear evidence that the reduction of Cu^{2+} to Cu^{+} after 1 hour in reduction gases at 278°C is a prerequisite for π-complexation bond forming. It is suggested that the sulfur adsorption capacities observed with Cu^{+} may be further enhanced by improving the conversion of Cu^{2+} to Cu^{+} in the reduction process. Takahashi *et al.* found that $CuCl_2/Al_2O_3$ can be reduced to $CuCl/Al_2O_3$ at 270°C for 1 hour in the presence of 5.3% H_2 in He. It is also in agreement with the above result from TPR as shown in Figure 4.1, that Cu^{2+} to Cu^{+} can be reduced at 278°C for 1 hour in presence of 10% H_2 in Ar.

The comparison of sulfur adsorption capacities from Cu^{+} impregnated on mesoporous alumina reduced with 2 gases, He and H_2, was shown that Cu^{+} reduced by H_2 (0.0095 mmol DBT/g) has higher breakthrough capacities than Cu^{+} reduced by He (0.0000 mmol DBT/g). This result was in parallel with TPR result obtained from reduction of Cu^{2+} by using He as shown in Figure 4.3. Subsequently, H_2 is the appropriate gas for reduction Cu^{2+} to Cu^{+}.

4.2.6 Comparison of the Sulfur Adsorption Capacities with Different Types of Sulfur Compounds

The two types of sulfur compounds, 150 ppm of dibenzothiophene and 4,6-dimethyldibenzothiophene were used in these experiments. The experiments were carried out at 0.4 cm^3/min, 60°C, and 100-400 μm of diameter size for Ni^{2+} impregnated on mesoporous alumina and 0.4 cm^3/min, 90°C, and 100-400 μm for Cu^+ impregnated on mesoporous alumina.

The results from breakthrough experiments of Ni^{2+} impregnated on mesoporous alumina are shown in Figure 4.13. Table 4.14 summarises the results from breakthrough and adsorption capacities.

Table 4.14 Breakthrough and adsorption capacities loading for dibenzothiophene and 4,6-dimethyldibenzothiopheme from simulated diesel fuel in Ni^{2+} impregnated on mesoporous alumina

Sulfur compound	Breakthrough capacity (mmol/g)	Adsorption capacity (mmol/g)
Dibenzothiophene	0.0199	0.0243
4,6-dimethyldibenzothiophene	0.0069	0.0179

From Figure 4.13 and Table 4.14, the breakthrough capacities of dibenzothiophene and 4,6-dimethyldibenzothiophene were 0.0199 mmol DBT/g and 0.0069 mmol 4,6-DMDBT/g, respectively. The breakthrough amount of dibenzothiophene was 3.3 times higher than that of 4,6-dimethyldibenzothiophene. The adsorption capacities were 0.0241 mmol DBT/g and 0.0156 mmol 4,6-DMDBT/g. The breakthrough and adsorption capacities of 4,6-DMDBT was lower than that for dibenzothiophene due to methyl groups on the 4- and 6-position of DMDBT, which strongly inhibit the adsorption of 4,6-DMDBT. Since the two methyl groups in 4,6-DMDBT are adjacent to the sulfur atom, it is reasonable to infer that a direct and π-

complexation interaction between the sulfur atom and the surface of the adsorbent might play an important role in the selective adsorption of sulfur compounds and the two methyl groups at the 4- and 6-positions may also hinder the approach of the sulfur atom to the surface.

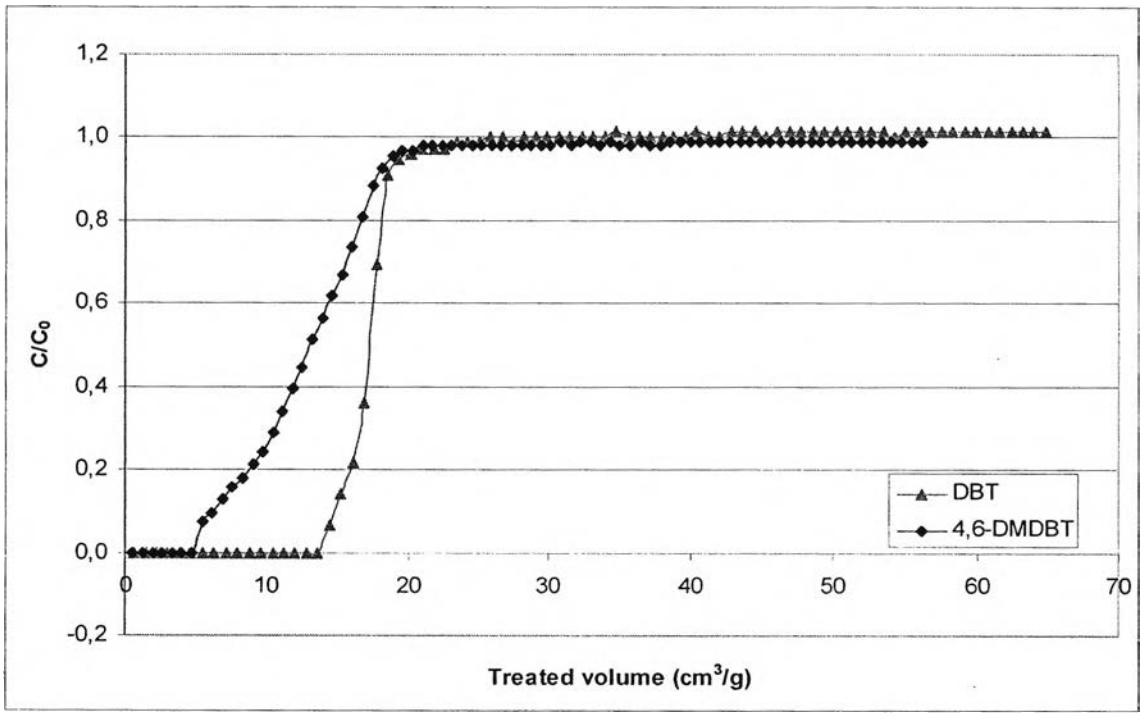

Figure 4.13 Breakthrough curve of Ni^{2+} impregnated on mesoporous alumina over dibenzothiophene, DBT (▲) and 4,6-dimethyldibenzothiophene, 4,6-DMDBT (♦).

The results from breakthrough experiments of Cu^{+} impregnated on mesoporous alumina are shown in Figure 4.14. Table 4.15 summarises the results from breakthrough and adsorption capacities.

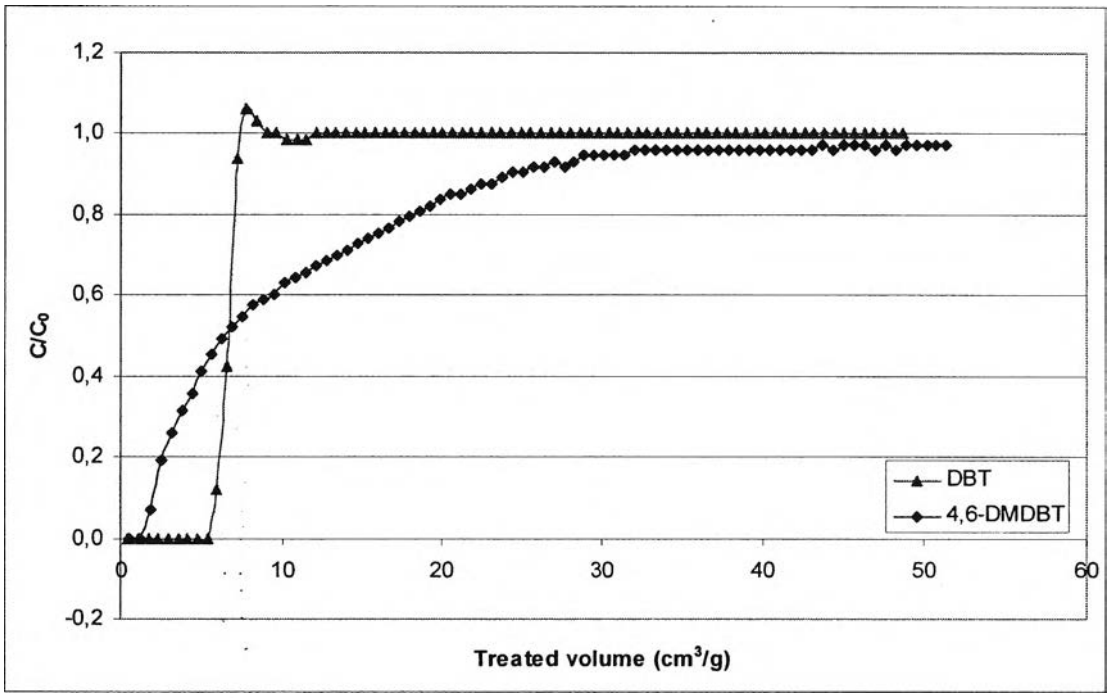

Figure 4.14 Breakthrough curve of Cu^{+} impregnated on mesoporous alumina over dibenzothiophene, DBT (▲) and 4,6-dimethyldibenzothiophene, 4,6-DMDBT (♦).

Table 4.15 Breakthrough and adsorption capacities loading for dibenzothiophene and 4,6-dimethyldibenzothiopheme from simulated diesel fuel in Ni^{2+} impregnated on mesoporous alumina

Sulfur compound	Breakthrough capacity (mmol/g)	Adsorption capacity (mmol/g)
Dibenzothiophene	0.0078	0.0089
4,6-dimethyldibenzothiophene	0.0004	0.0140

From Figure 4.14 and Table 4.15, the breakthrough capacities of dibenzothiophene and 4,6-dimethyldibenzothiophene were 0.0078 mmol DBT/g and 0.0004 mmol 4,6-DMDBT/g, respectively. The breakthrough amount of

dibenzothiophene was 20 times higher than that of 4,6- DMDBT. The adsorption capacities were 0.0089 mmol DBT/g and 0.0140 mmol 4,6-DMDBT/g. The breakthrough and adsorption capacities of 4,6- DMDBT was much lower than that for dibenzothiophene due to the same reason as above result. To compare the breakthrough and adsorption capacities of 4,6- DMDBT between Ni^{2+} and Cu^{+} impregnated on mesoporous alumina, Ni^{2+} impregnated on mesoporous alumina had higher amount of both capacities than Cu^{+} impregnated on mesoporous alumina.

4.2.7 Comparison of the Sulfur Adsorption Capacities in the Presence of Polyaromatics Compounds

The two types of polyaromatic compounds, 7% of naphthalene and 0.4% of phenanthrene were used in these experiments to compare adsorption capacities in case of presence of polyaromatic compounds in the simulated diesel. The simulated diesel contained 72.6% of n-dodecane, 20% of paradiethylbenzene, and 150 ppm of dibenzothiophene. The experiments were carried out at 0.4 cm^3/min, 60°C, and 100-400 μm of diameter size for Ni^{2+} impregnated on mesoporous alumina and 0.4 cm^3/min, 90°C, and 100-400 μm for Cu^{+} impregnated on mesoporous alumina.

The results from breakthrough experiments of Ni^{2+} impregnated on mesoporous alumina are shown in Figure 4.15 and Table 4.16 summarises the results from breakthrough and adsorption capacities.

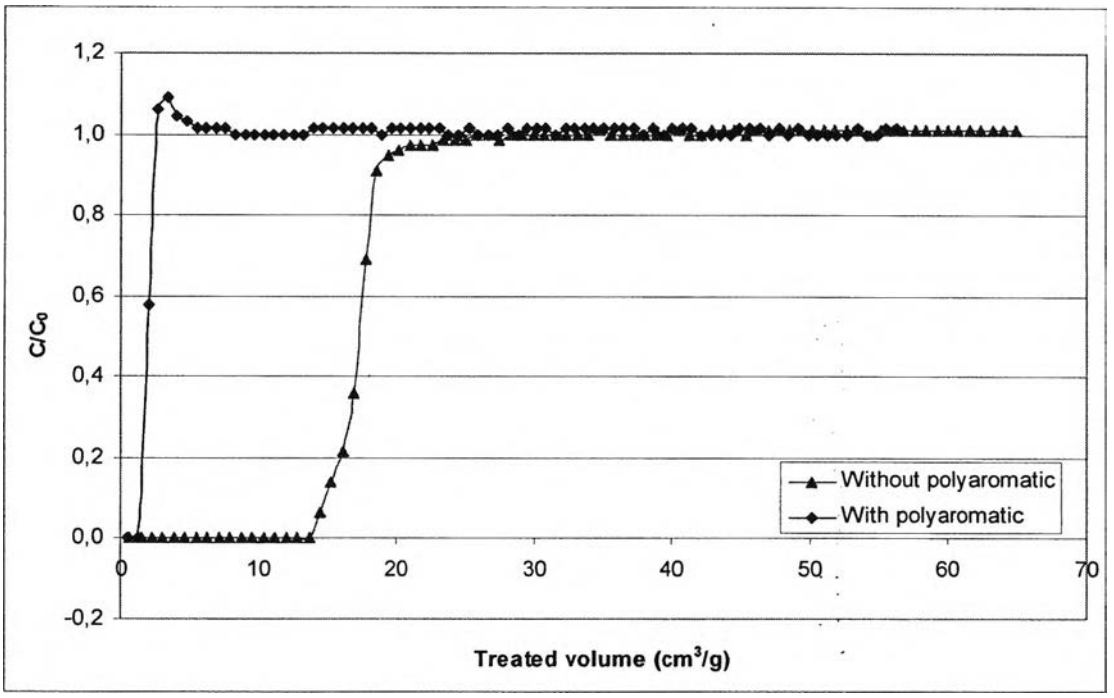

Figure 4.15 Breakthrough curve of dibenzothiophene in a fixed-bed adsorber over Ni^{2+} impregnated on mesoporous alumina without polyaromatic (▲) and with polyaromatic (♦).

Table 4.16 Breakthrough and adsorption capacities loading for dibenzothiophene, from simulated diesel fuel in Ni^{2+} impregnated on mesoporous alumina

Simulated diesel	Breakthrough capacity (mmol/g)	Adsorption capacity (mmol/g)
Without polyaromatic	0.0199	0.0243
With polyaromatic	0.0019	0.0019

From Figure 4.15 and Table 4.16, the breakthrough and adsorption capacities of dibenzothiophene in presence of polyaromatic compounds were 0.0019 mmol DBT/g. It can be seen that the breakthrough and adsorption capacities of

dibenzothiophene in presence of polyaromatic were much less than the breakthrough and adsorption capacities of dibenzothiophene without polyaromatic compounds, due to an adsorption competition between dibenzothiophene, naphthalene and phenanthrene. The polyaromatic compounds could be competitors because they have a quite similar structure as dibenzothiophene, as shown in Figure 4.16. Thus in presence of polyaromatic compounds, the sulfur breakthrough capacities were reduced 90% of the sulfur breakthrough capacities without polyaromatic compounds.

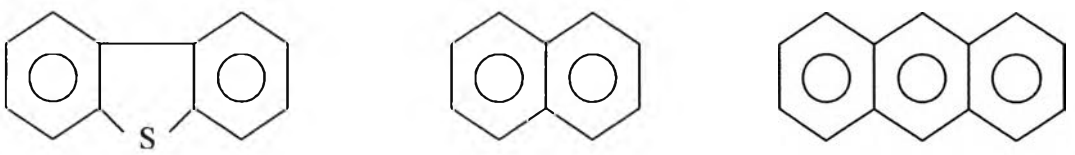

(a) Dibenzothiophene (b) Naphthalene (c) Phenanthrene

Figure 4.16 The structure of dibenzothiophene (a), naphthalene (b), and phenanthrene (c).

The brakthrough curves of five species, n-dodecane, paradiethylbenzene, dibenzothiophene, naphthalene and phenanthrene, over Ni^{2+} impregnated on mesoporous alumina are shown in Figure 4.17. The first breakthrough compound was naphthalene at 0.0969 mmol naphthalene/g. The second breakthrough compounds were dibenzothiophene at 0.0019 mmol DBT/g and phenanthrene at 0.0091 mmol phenanthrene/g . After breakthrough of paradiethylbenzene and dibenzothiophene, the C/C_0 value for these compounds increased sharply to over 1.0. It can be inferred from this phenomenon that the compounds have relatively lower adsorptive affinity than the subsequently breakthrough compounds, resulting in a displacement of the compounds with lower adsorptive affinity by the compounds with higher adsorptive affinity. Thus paradiethylbenzene and dibenzothiophene could be replaced by naphthalene and phenanthrene.

According to the breakthrough order, the adsorptive selectivity for the three adsorbates increases in order of naphthalene < dibenzothiophene ≈ phenanthrene. The breakthrough and adsorption capacities were shown in Table 4.16. In order to facilitate the quantitative discussion of the adsorptive selectivity, a relative selectivity factor was used in the present study, which is defined as:

$$\alpha_{i-n} = \frac{Cap_i}{Cap_n} \tag{1}$$

where Cap_i is the breakthrough capacities of compound i and Cap_n is the breakthrough capacities of the reference compound, naphthalene. The calculated relative selectivity factors on the basis of breakthrough curves are shown in Table 4.17. The relative selectivity is 1.00, 2.28 and 2.28 for naphthalene, dibenzothiophene and phenanthrene.

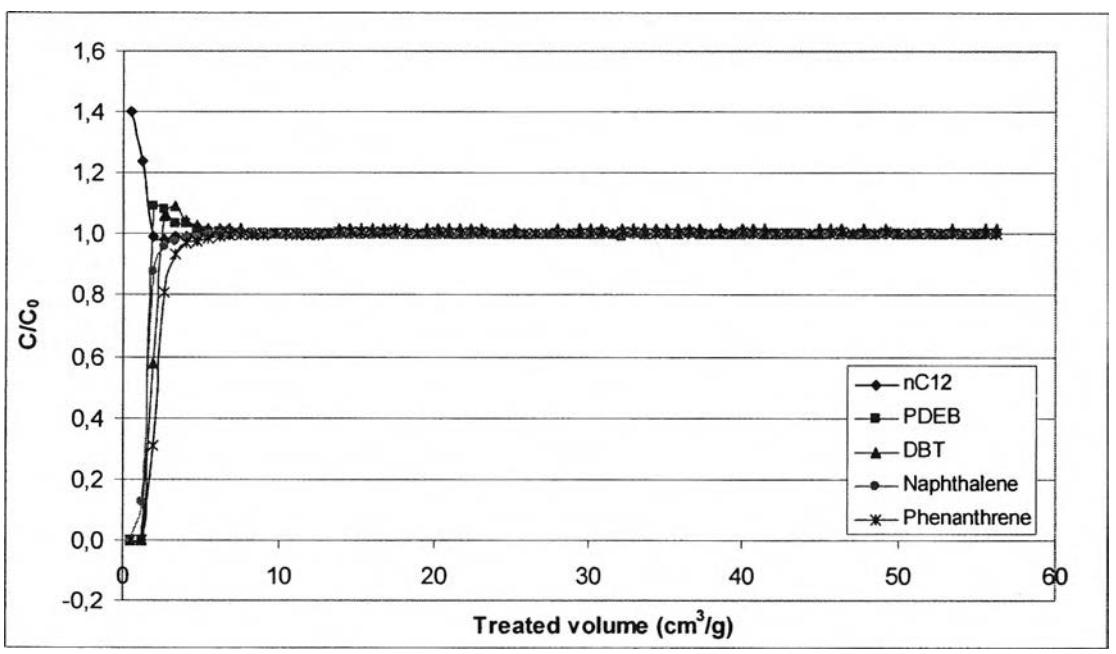

Figure 4.17 Breakthrough curve of all components in a fixed-bed adsorber over Ni^{2+} impregnated on mesoporous alumina.

Table 4.17 Breakthrough and adsorption capacities loading for dibenzothiophene, naphthalene and phenanthrene from simulated diesel fuel including polyaromatic in Ni^{2+} impregnated on mesoporous alumina

Compound	Breakthrough capacity (mmol/g)	Adsorption capacity (mmol/g)	Relative selectivity
Dibenzothiophene	0.0019	0.0019	2.28
Naphthalene	0.0969	0.2019	1.00
Phenanthrene	0.0091	0.0126	2.28

The results from breakthrough experiments of Cu^{+} impregnated on mesoporous alumina are shown in Figure 4.18. Table 4.18 summarizes the results from breakthrough and adsorption capacities.

From Figure 4.18 and Table 4.18, the breakthrough and adsorption capacities of dibenzothiophene in presence of polyaromatic compounds were 0.0017 and 0.0048 mmol DBT/g, respectively. It can be seen that the breakthrough and adsorption capacities of dibenzothiophene in presence of polyaromatic were less than the breakthrough and adsorption capacities of dibenzothiophene without polyaromatic compounds, due to an adsorption competition between dibenzothiophene, naphthalene and phenanthrene. The polyaromatic compounds could be competitors as the same reason with the above result. In presence of polyaromatic compounds, the sulfur breakthrough capacities were reduced 78% of the sulfur breakthrough capacities without polyaromatic compounds. Although the sulfur adsorption capacities of Cu^{+} impregnated on mesoporous alumina decreased less than that of Ni^{2+} impregnated alumina, the breakthrough capacities of Ni^{2+} impregnated on mesoporous alumina was still higher than that of Cu^{+} impregnated on mesoporous alumina.

Table 4.18 Breakthrough and adsorption capacities loading for dibenzothiophene, from simulated diesel fuel in Cu^{+} impregnated on mesoporous alumina

Simulated diesel	Breakthrough capacity (mmol/g)	Adsorption capacity (mmol/g)
Without polyaromatic	0.0078	0.0089
With polyaromatic	0.0017	0.0048

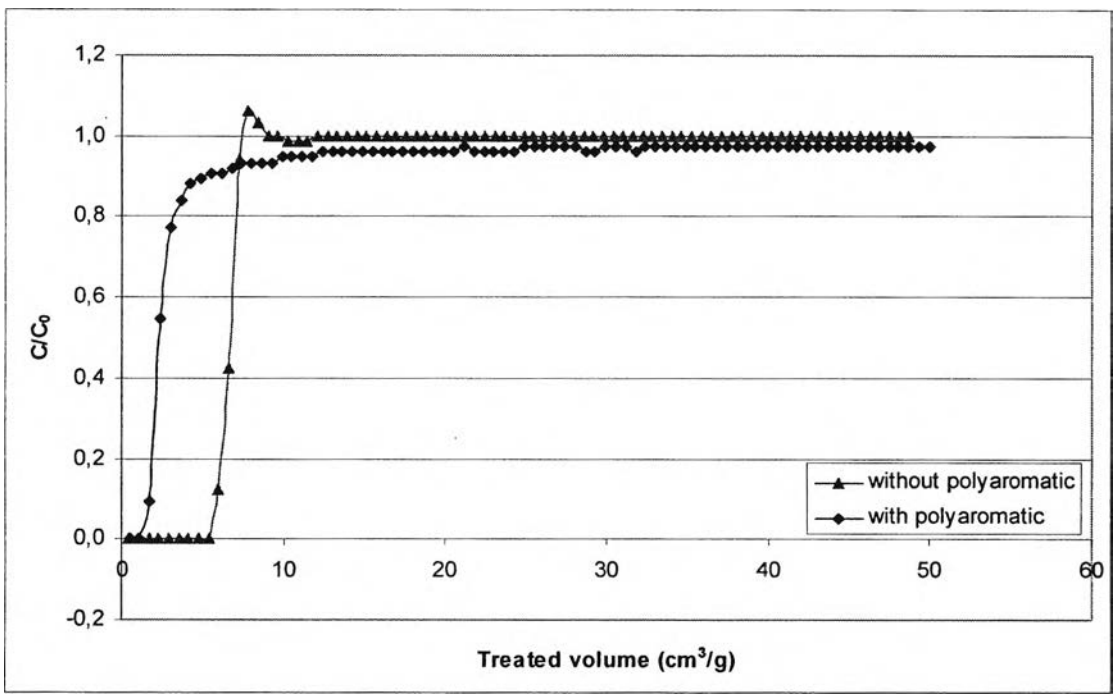

Figure 4.18 Breakthrough curve of dibenzothiophene in a fixed-bed adsorber over Cu^{+} impregnated on mesoporous alumina without polyaromatic (▲) and with polyaromatic (♦).

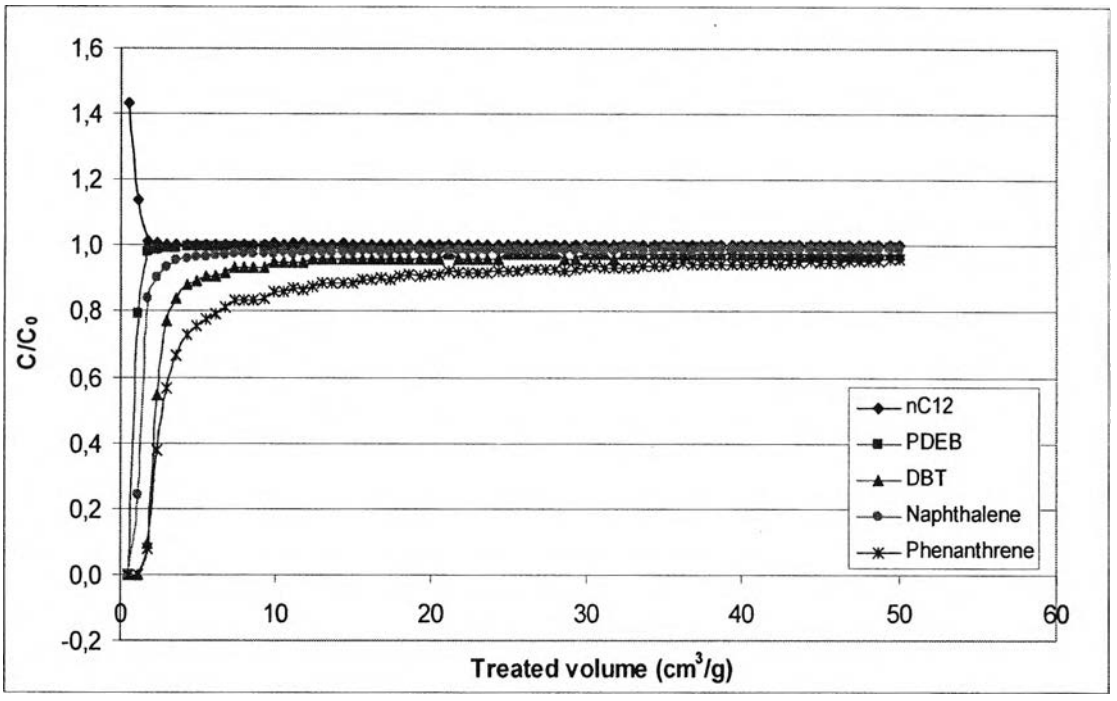

Figure 4.19 Breakthrough curve of all components in a fixed-bed adsorber over Cu^{+} impregnated on mesoporous alumina.

Table 4.19 Breakthrough and adsorption capacities loading for dibenzothiophene, naphthalene and phenanthrene from simulated diesel fuel including polyaromatic in Cu^{+} impregnated on mesoporous alumina

Compound	Breakthrough capacity (mmol/g)	Adsorption capacity (mmol/g)	Relative selectivity
Dibenzothiophene	0.0017	0.0048	2.27
Naphthalene	0.0862	0.2628	1.00
Phenanthrene	0.0081	0.0399	2.27

The breakthrough curves of five species, n-dodecane, paradiethylbenzene, dibenzothiophene, naphthalene and phenanthrene, over Cu^{+} impregnated on mesoporous alumina are shown in Figure 4.19. The first breakthrough compound was naphthalene at 0.0862 mmol naphthalene/g. The second two compounds were dibenzothiophene and phenanthrene at 0.0017 mmol DBT/g and 0.0081 mmol phenanthrene/g, respectively. According to the breakthrough order, the adsorptive selectivity for three adsorbates increases in order of naphthalene < dibenzothiophene ≈ phenanthrene. The calculated relative selectivity factors on the basis of breakthrough curves are shown in Table 4.19. The relative selectivity is 1.00, 2.27 and 2.27 for naphthalene, dibenzothiophene and phenanthrene.

4.2.8 Comparison of the Sulfur Adsorption Capacities in the Presence of Nitrogen Compounds

The two types of nitrogen compounds, 75 ppm of carbazole and 75 ppm of acridine were used in these experiments to see the influence of nitrogen compounds on the sulfur adsorption capacities. The simulated diesel contained 80% of n-dodecane, 20% of paradiethylbenzene, and 150 ppm of dibenzothiophene. The experiments were carried out at 0.4 cm^3/min, 60°C, and 100-400 μm of diameter size for Ni^{2+} impregnated on mesoporous alumina and 0.4 cm^3/min, 90°C, and 100-400 μm for Cu^{+} impregnated on mesoporous alumina.

The results from breakthrough experiments of Ni^{2+} impregnated on mesoporous alumina are shown in Figure 4.20 and Table 4.20 summarises the results from breakthrough and adsorption capacities.

From Figure 4.20 and Table 4.20, the breakthrough and adsorption capacities of dibenzothiophene in presence of nitrogen compounds were 0.0008 and 0.0018 mmol DBT/g, respectively. It can be seen that the breakthrough and adsorption capacities of dibenzothiophene in presence of nitrogen compounds were much less than the breakthrough and adsorption capacities of dibenzothiophene without nitrogen compounds, due to an adsorption competition among dibenzothiophene, carbazole and acridine. The nitrogen compounds can be competitors because they have a similar

structure as dibenzothiophene, as shown in Figure 4.21. Based on their structure, sulfur compounds are apparently bulkier than nitrogen compounds so it is more difficult for sulfur compounds to diffuse into inner parts of the adsorbent. Thus in presence of nitrogen compounds, the sulfur breakthrough capacities were reduced 96% of the sulfur breakthrough capacity without nitrogen compounds.

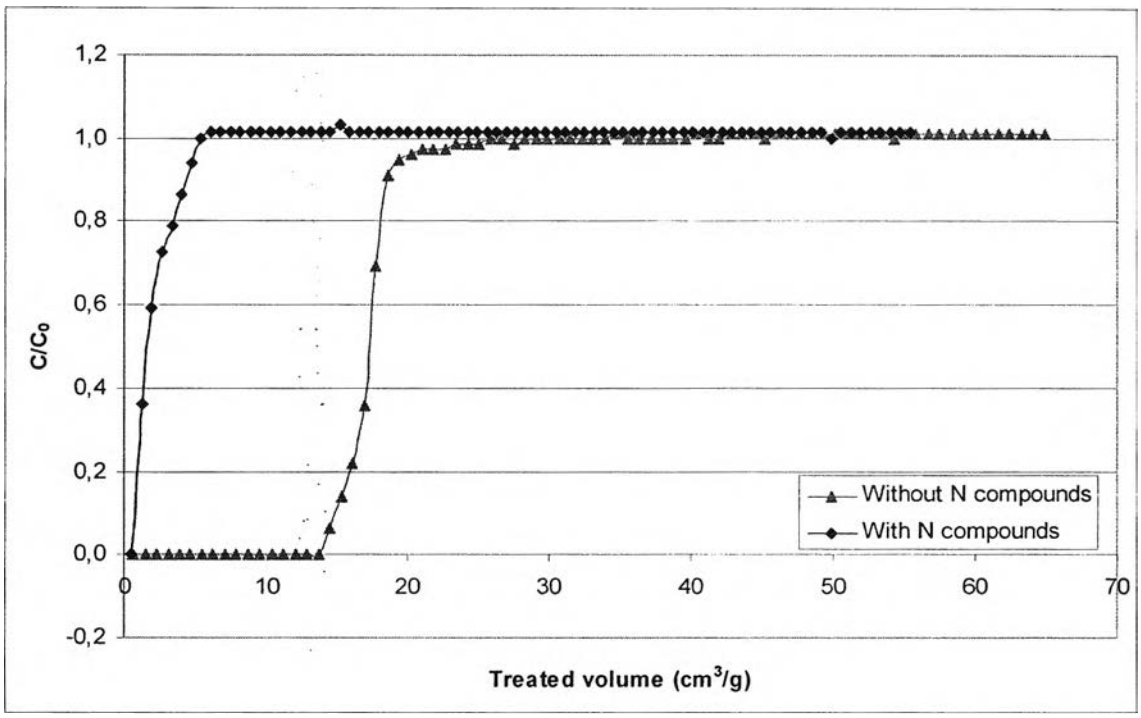

Figure 4.20 Breakthrough curve of dibenzothiophene in a fixed-bed adsorber over Ni^{2+} impregnated on mesoporous alumina without nitrogen compounds (▲) and with nitrogen compounds (♦).

Table 4.20 Breakthrough and adsorption capacities loading for dibenzothiophene, from simulated diesel fuel in Ni^{2+} impregnated on mesoporous alumina

Simulated diesel	Breakthrough capacity (mmol/g)	Adsorption capacity (mmol/g)
Without N compounds	0.0199	0.0243
With N compounds	0.0008	0.0018

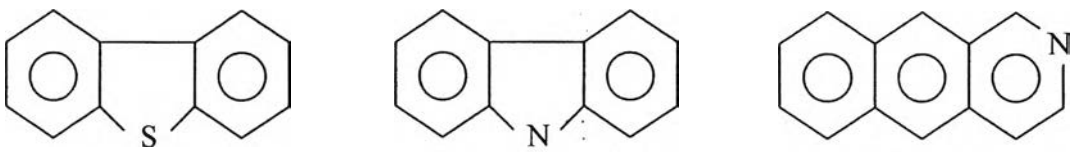

(a) Dibenzothiophene (b) Carbazole (c) Acridine

Figure 4.21 The structure of dibenzothiophene (a), carbazole (b), and acridine (c).

The breakthrough curves of five species, n-dodecane, paradiethylbenzene, dibenzothiophene, carbazole and acridine, over Ni^{2+} impregnated on mesoporous alumina are shown in Figure 4.22. The first breakthrough compound was dibenzothiophene at 0.0008 mmol DBT/g. The second compound was carbazole at 0.0105 mmol carbazole/g. The third breakthrough compound was acridine at 0.0334 mmol acridine/g. According to the breakthrough order, the adsorptive selectivity for the three adsorbates increases in order of dibenzothiophene < carbazole < acridine. The breakthrough and adsorption capacities were shown in Table 4.21. In order to facilitate the quantitative discussion of the adsorptive selectivity, a relative selectivity factor was used in the present study, which is the same as previous, except using dibenzothiophene as a reference compound. The calculated relative selectivity factors on the basis of breakthrough curves are shown in Table 4.21. The relative selectivity is 1.00, 8.65 and 35.42 for dibenzothiophene, carbazole and acridine.

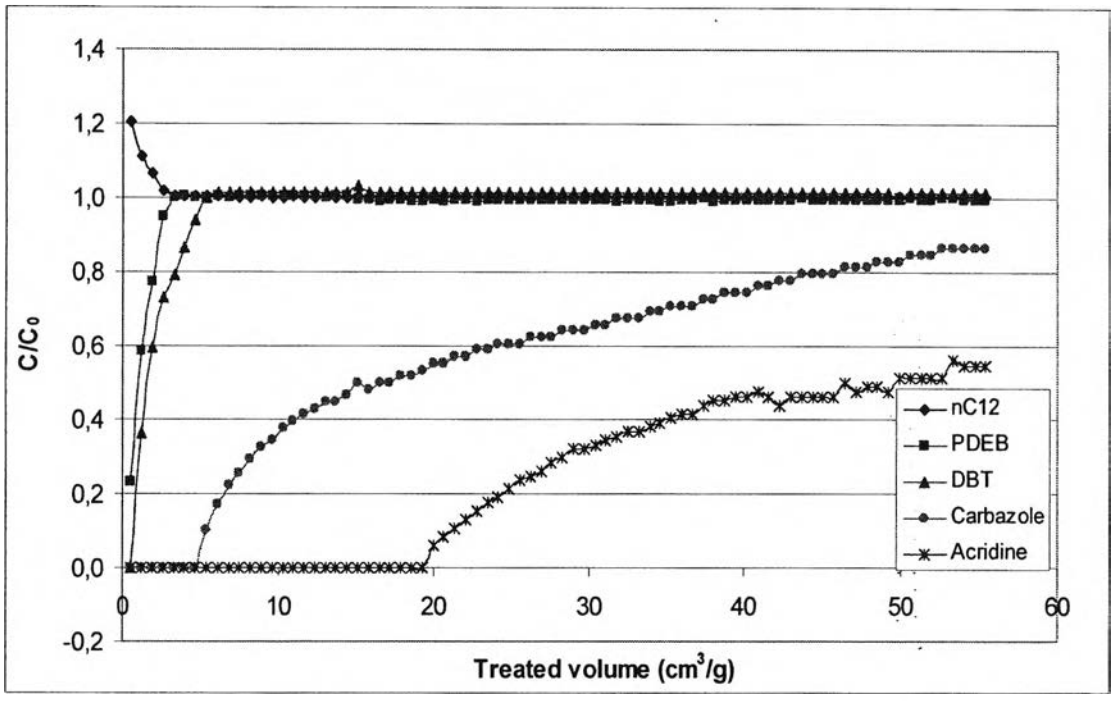

Figure 4.22 Breakthrough curve of all components in a fixed-bed adsorber over Ni^{2+} impregnated on mesoporous alumina.

Table 4.21 Breakthrough and adsorption capacities loading for dibenzothiophene, carbazole and acridine from simulated diesel fuel including nitrogen compounds in Ni^{2+} impregnated on mesoporous alumina

Compound	Breakthrough capacity (mmol/g)	Adsorption capacity (mmol/g)	Relative selectivity
Dibenzothiophene	0.0008	0.0018	1.00
Carbazole	0.0105	0.0437	8.65
Acridine	0.0334	0.0495	35.42

The results from breakthrough experiments of Cu^{+} impregnated on mesoporous alumina are shown in Figure 4.23 and Table 4.22 summarises the results from breakthrough and adsorption capacities.

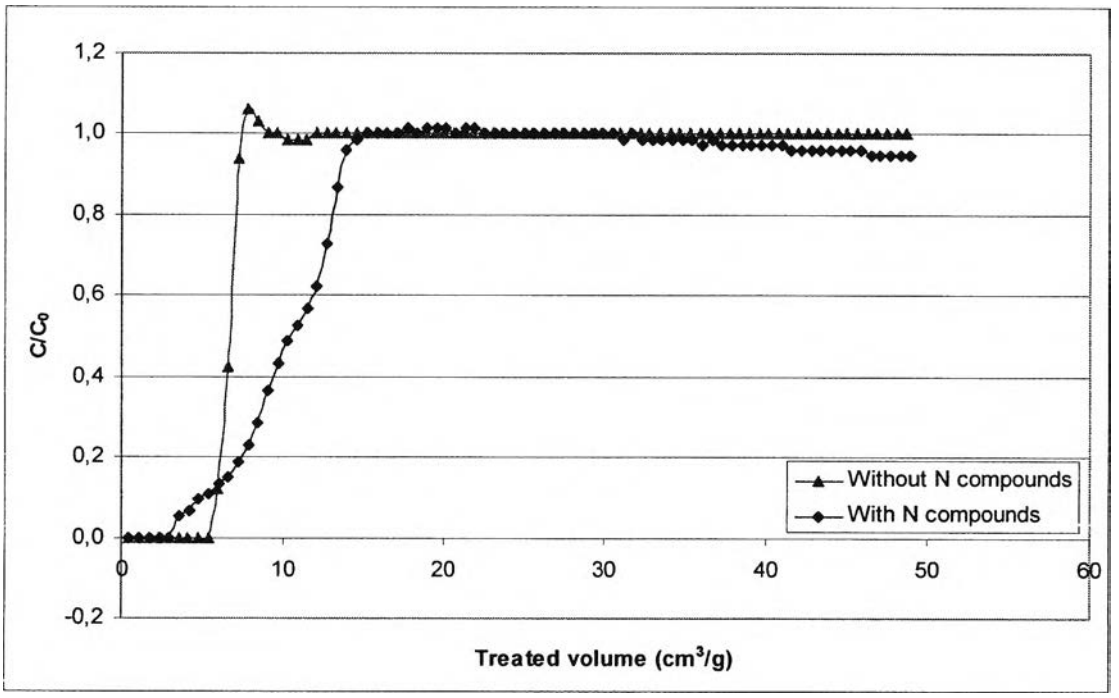

Figure 4.23 Breakthrough curve of dibenzothiophene in a fixed-bed adsorber over Cu^{+} impregnated on mesoporous alumina without nitrogen compounds (▲) and with nitrogen compounds (♦).

Table 4.22 Breakthrough and adsorption capacities loading for dibenzothiophene, from simulated diesel fuel in Cu^{+} impregnated on mesoporous alumina

Simulated diesel	Breakthrough capacity (mmol/g)	Adsorption capacity (mmol/g)
Without N compounds	0.0078	0.0089
With N compounds	0.0044	0.0154

From Figure 4.23 and Table 4.22, the breakthrough and adsorption capacities of dibenzothiophene in presence of nitrogen compounds were 0.0044 and 0.0154 mmol DBT/g, respectively. It can be seen that the breakthrough and adsorption capacities of dibenzothiophene in presence of nitrogen compounds were less than the breakthrough and adsorption capacities of dibenzothiophene without nitrogen compounds due to the same reason as above result. Thus in presence of nitrogen compounds, the sulfur breakthrough capacities were reduced 44% of the sulfur breakthrough capacity without nitrogen compounds. To compare the breakthrough and adsorption capacities between Ni^{2+} and Cu^{+} impregnated on mesoporous alumina, Cu^{+} impregnated on mesoporous alumina had higher both breakthrough and adsorption capacities than Ni^{2+} impregnated on mesoporous alumina.

The breakthrough curves of five species, n-dodecane, paradiethylbenzene, dibenzothiophene, carbazole and acridine, over Cu^{+} impregnated on mesoporous alumina are shown in Figure 4.24. The first breakthrough compound was dibenzothiophene at 0.0044 mmol DBT/g. The second compound was carbazole at 0.0613 mmol carbazole/g. For acridine, it was not observed a breakthrough point. It could be seen that all of acridine molecules were adsorbed on the adsorbent due to the very strong interaction between nitrogen atom of acridine and Cu^{+} atom on the adsorbent. According to the breakthrough order, the adsorptive selectivity for the three adsorbates increases in order of dibenzothiophene < carbazole < acridine. The breakthrough and adsorption capacities were shown in Table 4.23. The calculated

relative selectivity factors on the basis of breakthrough curves are shown in Table 4.23. The relative selectivity is 1.00, 9.36 and higher than 16.68 for dibenzothiophene, carbazole and acridine, respectively.

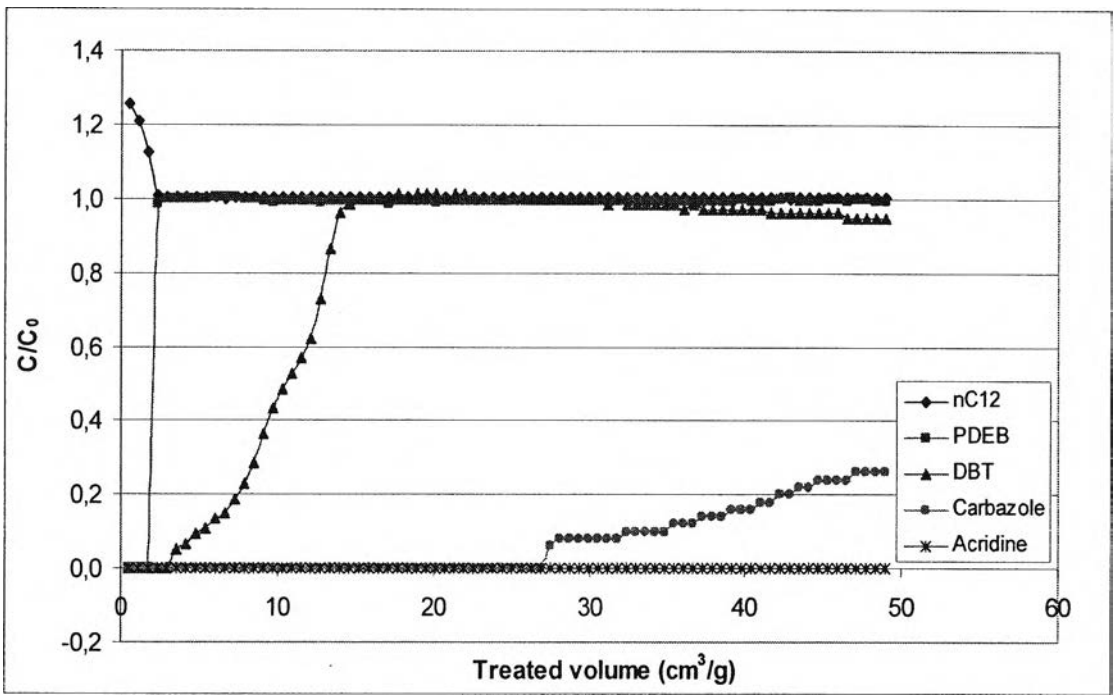

Figure 4.24 Breakthrough curve of all components in a fixed-bed adsorber over Cu^{+} impregnated on mesoporous alumina.

Table 4.23 Breakthrough and adsorption capacities loading for dibenzothiophene, carbazole and acridine from simulated diesel fuel including nitrogen compounds in Cu^{+} impregnated on mesoporous alumina

Compound	Breakthrough capacity (mmol/g)	Adsorption capacity (mmol/g)	Relative selectivity
Dibenzothiophene	0.0044	0.0154	1.00
Carbazole	0.0613	0.1016	9.36
Acridine	>0.0846	>0.0849	>16.68

From all of the above results, at feed flow rate of 0.4 cm^3/min and 60°C for Ni^{2+} impregnated on the adsorbent and 90°C and Cu^{+} impregnated on the adsorbent show higher breakthrough capacity. The breakthrough capacity of DBT was higher than 4,6-DMDBT for both of Ni^{2+} and Cu^{+} impregnated on mesoporous alumina. Moreover, the breakthrough capacity of DBT without polyaromatics and nitrogen compounds was higher than that with polyaromatics and nitrogen compounds.